Superconductor Science and Technology

PAPER

High-quality *in situ* fabricated Nb Josephson junctions with black phosphorus barriers

To cite this article: Wei Chen *et al* 2019 *Supercond. Sci. Technol.* **32** 115005

View the article online for updates and enhancements.

IOP ebooks™

Bringing together innovative digital publishing with leading authors from the global scientific community.

Start exploring the collection–download the first chapter of every title for free.

This content was downloaded from IP address 218.104.127.245 on 10/09/2021 at 14:18

IOP Publishing Superconductor Science and Technology
Supercond. Sci. Technol. 32 (2019) 115005 (7pp) https://doi.org/10.1088/1361-6668/ab3dc7

High-quality *in situ* fabricated Nb Josephson junctions with black phosphorus barriers

Wei Chen[1], Zuyu Xu[1], Wanghao Tian[1], Yangyang Lv[1], Mei Yu[1], Xianjing Zhou[1], Xuecou Tu[1], Jingbo Wu[1], Jun Li[1], Songlin Li[1], Biaobing Jin[1], Weiwei Xu[1], Dieter Koelle[2], Reinhold Kleiner[2,3], Huabing Wang[1,3] and Peiheng Wu[1]

[1] School of Electronic Science and Engineering, Nanjing University, Nanjing 210093, People's Republic of China
[2] Physikalisches Institut and Center for Quantum Science in LISA$^+$, Universität Tübingen, D-72076 Tübingen, Germany

E-mail: kleiner@uni-tuebingen.de and hbwang@nju.edu.cn

Received 10 June 2019, revised 13 August 2019
Accepted for publication 22 August 2019
Published 23 September 2019

Abstract

Owing to appealing physical properties such as broad tunability in bandgaps and structural anisotropy, black phosphorus (BP) holds great potential in exploring novel electronic devices. However, it is extremely challenging to use BP to fabricate electronic devices, since it is prone to deteriorate in air. To address this challenge, we demonstrate an *in situ* fabrication technique which enables us to minimize interfacial degradation and to fabricate vertical Josephson junctions by employing few-layer BP as a barrier between two closely spaced Nb electrodes. The current–voltage characteristics of the junctions are hysteretic at low temperatures and become nonhysteretic when approaching the junction critical temperature. In the resistive state the differential conductance increases with decreasing voltage. Microwave-induced Shapiro steps were observed, confirming the presence of the ac Josephson effect. We present different models to analyze the current–voltage characteristics and conclude that resistive state of the current–voltage characteristics points to a zero bias anomaly, which is presumably caused by Andreev reflections. Our *in situ* fabrication technique represents a viable way to incorporate air-unstable materials for electronics and offer a chance to explore their unique functionalities.

Supplementary material for this article is available online

Keywords: Josephson junction, black phosphorus, two-dimensional (2D) materials, *in situ* fabrication

(Some figures may appear in colour only in the online journal)

1. Introduction

Due to their unique electronic properties, Josephson junctions play an essential role in superconducting electronics, most recently in the context of quantum computing [1–6]. The junction barrier, which can be basically an insulator, a semiconductor, or a metal, plays a critical role in determining the overall junction properties and functionalities. For example, a barrier that is sensitive to light provides the possibility of fabricating optically tunable superconducting junctions [7]. Hence, the barrier has been a major focus of interest in this field of research. Recently, two-dimensional layered materials are extensively studied as the barrier layer for making Josephson devices, due to their atomic thickness and flatness. The well-controlled thickness (down to a monolayer) and the high interface cleanness offer advantages in fabricating high-quality devices with new physics and elevated performance [8–12].

Black phosphorus (BP), similar to bulk graphite, is a layered structure in which individual atomic layers of the

[3] Authors to whom any correspondence should be addressed.

 © 2019 IOP Publishing Ltd Printed in the UK

puckered honeycomb lattices are stacked by van der Waals interactions [13]. Few-layer BP exhibits unique properties absent in other 2D structures. For example, BP has a strongly anisotropic conducting behavior and highly anisotropic optical and phonon properties [14, 15]. It also shows a large thickness-dependent bandgap tuning range from 0.3 eV (bulk) to ~2 eV (monolayer), filling the gap between zero-bandgap graphene and wide-bandgap 2D transition metal dichalcogenides (1.5–2.5 eV) [13]. With its peculiar properties, BP has attracted increasing interest for potential applications in thin-film electronics, mid- and near-infrared optoelectronics, and for the development of new-concept devices [15–17].

However, because BP is relatively active and will deteriorate rapidly in the air [18], there are few relevant studies on Josephson junction devices with BP as the barrier. Also, because of unknown interface properties between the superconducting electrodes and BP, it is very hard to predict the type of transport across the barrier, which can range from tunneling for a low-transparency barrier to ballistic transport for a high-transparency one. In this paper, we report on the development of an *in situ* fabrication process to minimize the interfacial degeneration of BP, which enables us to fabricate Josephson junctions by using few-layer BP as a barrier between two superconducting Nb electrodes. We will discuss resistance versus temperature (R–T), the temperature dependence of the junction critical current and the current–voltage curves from the Nb/BP/Nb Josephson junctions. All data indicate a good interface transparency. At temperatures down to 2.6 K, clear Shapiro steps under microwave irradiation at different frequencies were observed, at junction voltages satisfying the well-known Josephson relation. Now that BP has not only unique anisotropic photoelectric [14, 15] but also gate-tunable properties [19], Nb/BP/Nb junctions may pave a new way to study the characteristics of BP for new-concept superconductor electronics.

2. Sample fabrication

It is well known that a good interfacial contact between the barrier and the superconducting electrodes is extremely important for the successful fabrication of Josephson junctions. However, the few-layer BP barrier and the superconducting Nb electrodes are extremely prone to deteriorate in air. In order to employ the unique but chemically active material to create Nb/BP/Nb Josephson junctions, we devised an *in situ* fabrication system (AdNaNo-Tek Ltd), where a glovebox, reactive-ion etching, electron-beam deposition, and magnetron sputtering facilities are connected together. Since the connection tubes are in ultra-high-vacuum (UHV) condition ($<10^{-8}$ Torr), this *in situ* fabrication method ensures that the interface between BP and Nb is never exposed to air, and consequently interfacial degeneration is minimized dramatically.

Few-layer BP was obtained by cleaving bulk BP crystals (99.995%, Muke Nano) several times with the well-known adhesive tape method. BP can easily deteriorate in oxygen and moisture [18], so we mechanically exfoliated it in a glovebox with Ar atmosphere ($H_2O < 0.1$ ppm, $O_2 < 0.1$ ppm). To avoid degradation, we transferred BP flakes directly onto 40 nm thick Nb electrodes pre-patterned on sapphire or Si substrates via a dry-transfer method in the glovebox. Then, the as-prepared sample was quickly transferred through a UHV connection tube to an electron-beam evaporation system for Al deposition and then to a dc sputtering system for Nb deposition, to prepare the top electrode. A bilayer of Al (2 nm)/Nb (60 nm) was deposited onto the sample, followed by lithography to define (Al/Nb) electrodes on top of the BP. The evaporation rate of Al was about 0.8 Å s^{-1} and the evaporation rate of Nb was 1 Å s^{-1}. Note that during the deposition of Al, some amount of aluminum phosphate may have formed at the interface which may have an effect on the interface transparency. After developing the photoresist, reactive-ion etching was used to remove the undesired Nb surrounding the junctions by SF_6 milling. Then, the samples were put into alkaline solution for 2 s to remove the residual Al layer and immersed in alcohol for 1 min to eliminate the remaining alkaline solution. This process produces superconductor–BP–superconductor (S–BP–S) Josephson junctions on sapphire or Si substrates, with a typical vertical sandwich structure. Note that Al was used as a mask layer to avoid over-etching the BP and the bottom electrodes. In order to minimize the effect of degradation, the samples were immediately covered with polymethyl methacrylate (PMMA) and loaded into a cryogenic system with less than 20 min of exposure to air. Below we show data for one sample with a junction area of ~85 μm^2. The junction was patterned on a sapphire substrate and the thickness of the BP layer is about 4 nm (eight monolayers), as estimated by Raman spectra and atomic force microscopy. Other junctions behaved similarly.

Figure 1(a) shows a schematic view and figure 1(b) shows a scanning electron microscopy (SEM) image of the Josephson junction with BP as the barrier.

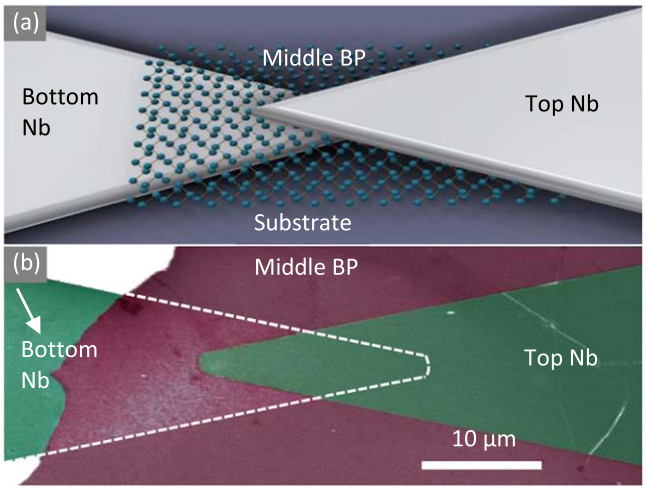

Figure 1. Nb/BP/Nb Josephson junction geometry. (a) Schematic view and (b) SEM image. In (b), the white dotted line outlines the bottom Nb electrode. The thickness of the BP barrier layer is about 4 nm (or eight monolayers), as estimated by Raman spectra and by atomic force microscopy.

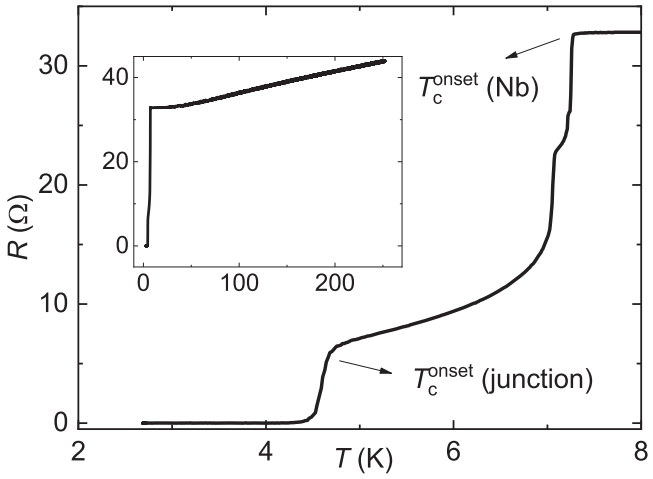

Figure 2. Resistance versus temperature (R–T) curve of the *in situ* fabricated junction (recorded with a bias current $I = 8$ μA) between 2.6 and 8 K. Inset: R–T curve in the full temperature range.

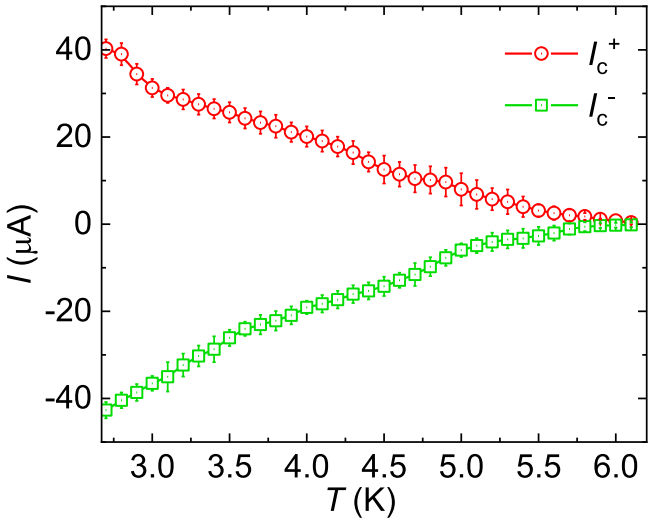

Figure 3. Junction critical current I_c as a function of bath temperature. Open circles are for a positive bias current and open squares are for negative bias. Error bars are indicated.

3. Results and discussion

Electrical transport measurements were carried out in a Gifford–McMahon-type refrigerator with temperatures down to 2.6 K. The measurement DC lines were equipped with RC filters to eliminate electrical noise. The electrical transport properties of the junction were measured by a standard four-terminal method with two separated contacts on each Nb electrode. Figure 2 shows the temperature dependence of the junction resistance R. Below 7.3 K the first Nb electrode and below 7 K the other Nb electrode becomes superconducting. The transition starting at 4.7 K arises from the junction. Zero resistance is reached below 4.5 K. For the measurement the bias current was set to 8 μA, thus zero resistance implies that the junction critical current exceeded 8 μA at 4.5 K. The inset shows a metallic resistance versus temperature (R–T) curve behavior above T_c of Nb, revealing a high-quality interfacial contact between BP and Nb electrodes due to the *in situ* fabrication process.

To further stress the importance of the *in situ* fabrication process, we make a comparison of the transport properties in junctions between the *in situ* and *ex situ* fabrication methods (see figure S1 available online at stacks.iop.org/SUST/32/115005/mmedia). By *ex situ,* we mean that we do not mechanically cleave BP in a glovebox or do not transfer the sample into the *in situ* fabrication system through the connection tube. Although we have made great efforts to reduce the air exposure time of the *ex situ* samples as much as possible, we could not obtain a BP-based Josephson junction with reasonable properties.

Figure 3 shows the junction critical current I_c as a function of bath temperature. Open circles are for a positive bias current and open squares are for negative bias. I_c increases about linearly with decreasing temperature, with a junction critical temperature of about 6.0 K. A roughly linear temperature dependence of I_c can be characteristic for Cooper pair tunnelling but can also be observed for ballistic transport [11, 20, 21]. Note that the critical current at 2.6 K is about 40 μA, corresponding to a critical current density of about 47 A cm^{-2}. This is relatively low but not an unusual value for Josephson junctions.

The progressive evolution of typical I–V curves with temperature is illustrated in figure 4, where the arrows represent the sweeping direction of the bias current. At $T = 2.6$ K, the I–V curve shows sharp and hysteretic switching between the zero-voltage state and the finite-voltage state. With increasing temperature, the hysteresis decreases and disappears when the junction critical temperature is approached. Note that the I–V curves show no indication of a gap structure which for Nb should appear near 2 mV. This strongly indicates that the resistive part of the I–V curves is not mainly due to tunneling. In the resistive state the differential resistance, although nonlinear, is on the order of 5–10 Ω, implying a resistance-times-area product of below 1 $\mu\Omega\,\mathrm{cm}^2$, which is at least three orders of magnitude lower than a typical value for a tunnel junction and indicates a good interface transparency. We also note that, when extrapolating the resistive part of the I–V curves back to zero voltage, there seems to be a substantial excess current.

In the following we discuss three models to fit the shape of the I–V curves shown in figure 4, the standard resistively and capacitively shunted junction (RCSJ) model for underdamped Josephson junctions [22], an RCSJ model coupled to heat diffusion equations and finally an RCSJ model with a nonlinear quasiparticle current. Only the latter model gives reasonable agreement with the data.

In the standard RCSJ model, which can describe many Josephson junctions in great detail, the I–V curves are calculated as the sum of the Josephson current, a displacement current and an ohmic quasiparticle current as

$$i = \beta_c \ddot{\gamma} + \dot{\gamma}/r + i_c \sin\gamma, \tag{1}$$

where $\beta_c = 2\pi I_{c0} R_0^2 C/\Phi_0$ is the Stewart–McCumber parameter, R_0 is the junction resistance, I_{c0} is the Josephson critical current and C is the junction capacitance. Φ_0 denotes the

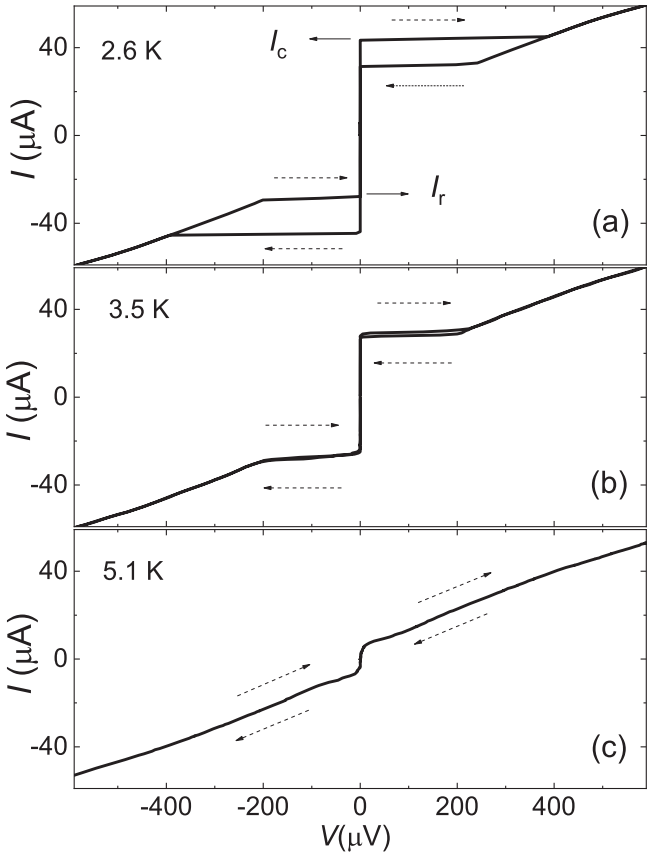

Figure 4. Current–voltage (*I–V*) curves of the *in situ* fabricated junction, measured at (a) 2.6 K, (b) 3.5 K, and (c) 5.1 K with increasing and decreasing bias current (indicated by dashed arrows). The critical current (I_c) and the retrapping current (I_r) are indicated in (a).

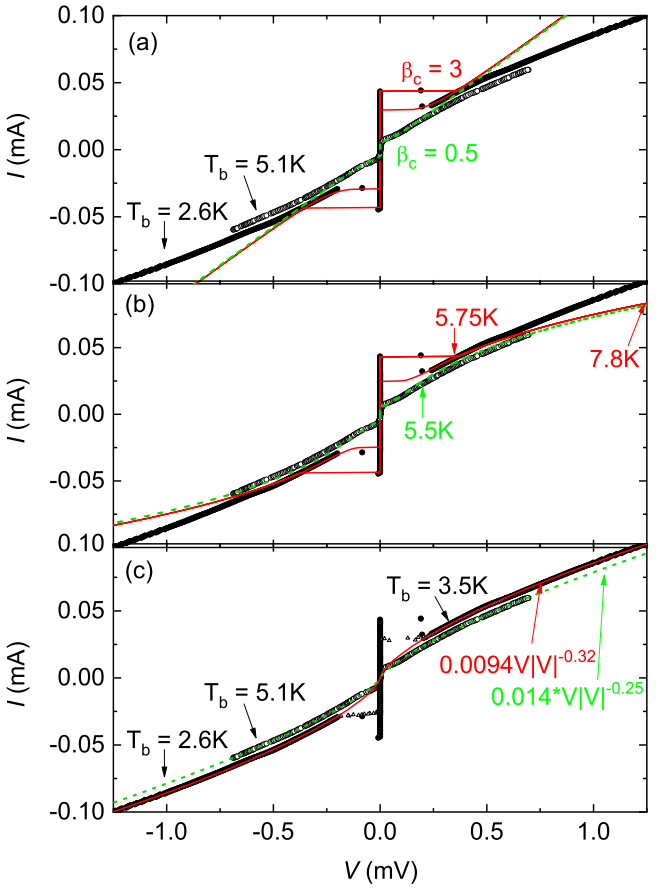

Figure 5. Models to fit the experimental *I–V* curves of figure 4: (a) standard RCSJ model, (b) RCSJ model coupled to heat diffusion equations, (c) power-law fits to the resistive branch of experimental *I–V* curves. In all graphs, experimental data for bath temperatures of 2.3 K (5.1 K) are shown by black solid (open) circles. In (c) in addition, 3.5 K data are included by open black triangles. In (a) and (b), fits to the 2.6 and 3.5 curves are shown by, respectively, solid red and green dashed lines. In (c) the fit to the 2.6 and 3.5 K curves are shown by the solid red line, the fit to the 5.2 K curve by the dashed green line. Numbers in (b) indicate some junction temperatures, as calculated in the thermal model.

flux quantum and γ is the Josephson phase difference. Currents are normalized to I_{c0}, resistances to R_0, voltages to $I_{c0}R_0$ and time to $\Phi_0/2\pi I_{c0}R_0$. In the standard notation i_c and r can be set to 1. Equation (1) yields the time dependent normalized voltage $v = \dot{\gamma}$. The voltage V used in the *I–V* curves is obtained by time averaging v. Figure 5(a) shows the best fits for the experimental *I–V* curves taken at, respectively 2.6 K and 5.1 K. The fit to the 2.6 K curve is shown by a red solid line. Here we used $\beta_c = 3$ to match the hysteresis. The fit to the 5.1 K curve, shown by the green dashed line, uses $\beta_c = 0.5$. The fits are very poor, for the reason that the experimental curves exhibit a negative curvature of the resistive branch, i.e. a differential resistance increasing with bias current. This feature may be indicative of a Joule heating effect, assuming that the junction resistance increases with temperature. In extreme cases the hysteresis in the *I–V* curves can be purely caused by heating [23].

To include heating, similar as in [24] we combine equation (1) with the heat diffusion equation

$$C_h\dot{T} = P - \int_{T_b}^{T} KdT, \qquad (2)$$

with the heat capacitance C_h of the junction, the thermal conductance K of the junction to the bath and the Joule power input $P = U^2/R$. T_b is the bath temperature (simply denoted as T in the main part of the text) and T is now the actual temperature of the junction. We assume that the junction resistance and the Josephson critical current are temperature dependent and use I_{c0} and R_0 as their values at some normalization temperature T_n (2.6 K for the simulations shown here). Thus, $i_c = I_c(T)/I_{c0}$ and $r = R(T)/R_0$ are temperature dependent functions. The temperature is calculated from equation (2) using the Joule power P generated from equation (1). For $I_c(T)$ we use a linear temperature dependence $I_c(T) \propto (1-T/T_{cJ})$, with $T_{cJ} = 6$ K, as suggested from figure 3. We obtain $R(T)$ by fitting the *R–T* curve shown in figure 2 over some temperature range above T_{cJ} and extrapolating it to some residual value below T_{cJ}. The fits are shown in figure 6. The first fit function is given by R (*T*) [Ω] = 4.2 + 0.023 (T [K])^3 and is close to the measured $R(T)$ curve for temperatures between T_{cJ} and 6.5 K. Below T_{cJ} the fit curve approaches the value of 4.2 Ω at low temperatures. The second fit function is given by R (*T*) [Ω] = 4.2 + 0.023

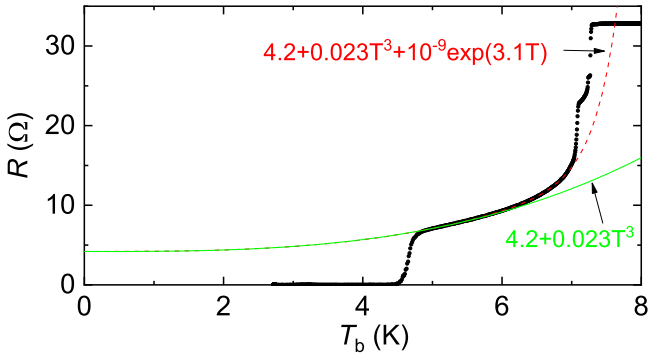

Figure 6. Fits (lines) to the measured (solid circles) temperature dependence of the junction resistance. For the fit formulas, the temperature T is in Kelvin and the output is in Ω.

(T [K])^3 + 10^{-9} exp(3.1 T[K]). This function basically coincides with the first fit function for temperatures below 6 K but follows the measured $R(T)$ curve up to about 7 K. As it is commonly done [25], we assume power laws in T for the thermal conductance, with powers between 1 and 5. The prefactor is adjusted so that the hysteresis in the I–V curves, as well as the resistive part of the I–V curves near the critical current, are reproduced. Figure 5(b) shows results for $K \propto T^5$, using the first fit function for $R(T)$. A power of 5 for $K(T)$ is in the range of Nb films at low temperature. Apparently, the fits do not agree with the measured I–V curves at high currents and voltages. Using the second fit function for $R(T)$ or using a power below 5 for the thermal conductance makes the fits even worse (not shown). In essence the crux is that, e.g., the resistance observed after switching to the resistive state at $T_b = 2.6$ K requires a junction temperature of 5.75 K and higher, resulting in the need to use a very low thermal conductance which for the fits shown amounts to 2.8 pW K^{-1} at $T_b = 2.6$ K. Using the Nb film thickness as the effective distance of the junction to the bath and a junction area of 85 μm one finds a thermal conductivity of about 1.3 mW mK^{-1}, which is at least four orders of magnitude below reported thermal conductivities of Nb near 2.6 K [25, 26]. One would have to increase the effective distance to bath to the mm scale to get reasonable values for thermal conductivities of either Nb or Si. We conclude that the thermal model cannot reproduce the measured I–V curves for reasonable model parameters.

The remaining possibility is that the quasiparticle conductance is nonlinear. Indeed, as shown in figure 5(c), the resistive parts of the I–V curves at 2.6 and 3.5 K can be described very well with $R^{-1} \propto |V|^{-0.32}$. For the 5.2 K curve, the power is somewhat lower, 0.25. The decrease of the differential resistance (increase of the differential conductance) for $V \to 0$ is reminiscent of a zero bias anomaly (ZBA), observed for many Josephson junctions. There can be various reasons for the formation of the ZBA [27], and multiple Andreev reflections is one of them [28]. To model the experimental I–V curves in the presence of a ZBA we replaced the ohmic quasiparticle current $\dot{\gamma}/r$ in equation (1) nonlinear dependence, making use of the $I/V \propto V^{-p}$ dependences introduced above. For the calculations, we use a

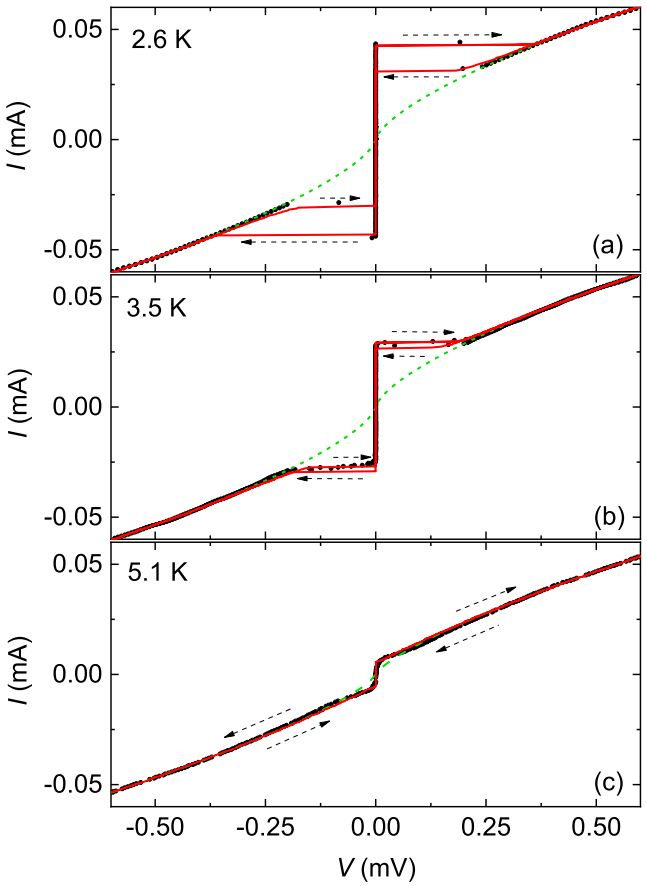

Figure 7. Fits to the experimental I–V curves of figure 4, as obtained from the RCSJ model with nonlinear quasiparticle current. Experimental data are shown by black solid circles, dashed green lines are the power-law fits of figure 5(c), solid red lines are the results of simulations using these power-law dependences as a nonlinear quasiparticle current in the RCSJ model.

McCumber parameter $\beta_c = 2\pi I_{c0} R_0^2 C/\Phi_0$ of 4.5, where R_0 is now the linearized resistance V/I at 44 μA, i.e. the 2.6 K critical current. We also include thermal fluctuations.

The results of the simulations using this RCSJ model with nonlinear quasiparticle current are shown in figure 7. The agreement with the experimental curves is reasonable. Also note that an opening of a ZBA below the transition temperature of the Nb electrodes ZBA could explain the 'metallic' behavior of $R(T)$ for temperatures below 7 K or so.

Direct experimental evidence of the genuine Josephson junction is provided by the microwave irradiation response. Applying a microwave of frequency f to the sample results in Shapiro steps in the I–V curve at discrete bias voltages $V_n = nhf/2e$ [29], where n is an integer and h is Planck's constant. The constant-voltage Shapiro steps can be attributed to the synchronization of the Josephson oscillations and the applied microwave radiation. Figure 8(a) shows I–V curves obtained from the *in situ* fabricated Nb/BP/Nb Josephson junction, irradiated by microwave of different frequencies. For I–V curves under microwave irradiation at 40 GHz, 35 GHz, 30 GHz, and 25 GHz, the current steps were observed at integer multiples of $\Delta V = 82.7$ μV, 72.4 μV, 61.7 μV, and 51.4 μV, respectively. As shown in figure 8(b)

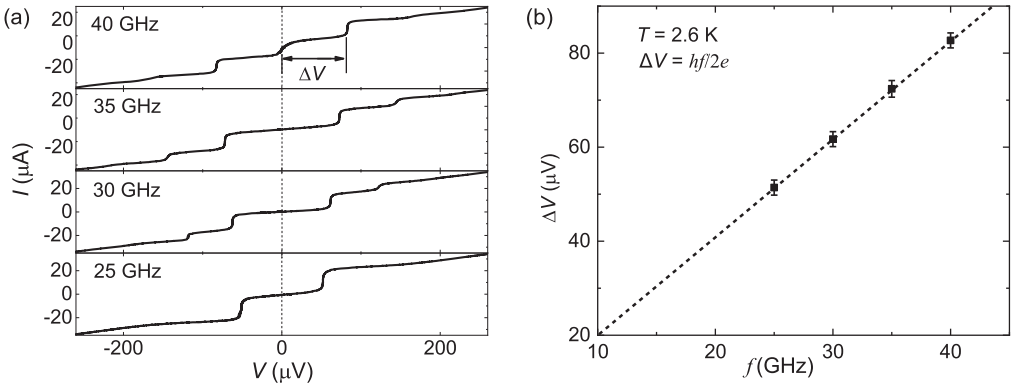

Figure 8. a.c. Josephson effect of the junction created by the *in situ* fabrication process, measured at $T = 2.6$ K. (a) *I*–*V* curves under microwave irradiation with different frequencies. (b) Interval ΔV versus irradiation frequency. Symbols and error bars represent the experimental values, the dotted line is given by $\Delta V = hf/2e$.

these values are very close to the ΔV values expected from the a.c. Josephson relation, $\Delta V = hf/2e$. In fact, we also tried to simulate the *I*–*V* curves under microwave irradiation. However, for all three approaches (conventional RCSJ, RCSJ with Joule heating and RCSJ with nonlinear quasiparticle current) there was no agreement with data. Both within the conventional and the nonlinear RCSJ simulations the junction behaved chaotic, and the observed Shapiro steps were too small and instable. For the RCSJ model coupled to heat diffusion equations, there was strong overheating and the Shapiro steps were by far too small. It is likely that one also needs to consider a non-sinusoidal Josephson current-phase relation to fully describe the data.

4. Conclusion

We have developed an *in situ* method to fabricate Nb/BP/Nb Josephson junctions. The junctions showed a metallic *R*–*T* curve behavior above T_c of Nb, pointing to good interfacial properties between Nb and BP. The *I*–*V* curves of the junctions exhibit hysteresis at low temperatures and become nonhysteretic when approaching the junction critical temperature. The junction critical current increases linearly with decreasing temperature. Well-behaved microwave-induced Shapiro steps were observed, confirming the presence of the ac Josephson effect. In the resistive state of the junctions, the differential conductance of the *I*–*V* curves increases with decreasing voltage, a feature which cannot be described within the standard RCSJ model. We have also ruled out Joule heating as the source for the large conductance at low voltages and conclude that resistive state of the *I*–*V* curves points to a zero bias anomaly which is presumably caused by Andreev reflections.

From a comparison of the transport properties in junctions between different fabrication methods, we found that the *in situ* method provides high-quality interfacial contact between BP and Nb electrodes, which is the key for fabricating robust junctions. The proposed *in situ* method is not limited to fabricating BP-based Josephson junctions but is readily applicable to a variety of air-sensitive devices. Last but not least, we stress that BP thin flakes have ambipolar insulator-to-metal transition properties by applying an electric field [19], the *in situ* fabrication will lead to a very crucial step towards the applications of gate-tunable BP-based Josephson devices.

Acknowledgments

We gratefully acknowledge financial support by the National Natural Science Foundation of China (Nos. 61727805, 61611130069, 61521001, 61771235, 61674080, and 61801209), the National Key R&D Program of China (2018YFA0209002 and 2017YFA0206304), Jiangsu Provincial Natural Science Fund (BK20160635), Nanjing University Innovation and Creative Program for PhD Candidate (CXCY17-15), the COST action NANOCOHYBRI (CA16218) and the Deutsche Forschungsgemeinschaft via project KL930-13/2.

ORCID iDs

Xianjing Zhou https://orcid.org/0000-0002-0137-7921
Jun Li https://orcid.org/0000-0002-6928-1256
Dieter Koelle https://orcid.org/0000-0003-3948-2433
Huabing Wang https://orcid.org/0000-0003-4802-6077

References

[1] Bergeal N *et al* 2010 *Nature* **465** 64
[2] Strambini E *et al* 2016 *Nat. Nanotechnol.* **11** 1055
[3] Macklin C *et al* 2015 *Science* **350** 307
[4] Simmonds R W *et al* 2004 *Phys. Rev. Lett.* **93** 077003
[5] Fornieri A, Timossi G, Virtanen P, Solinas P and Giazotto F 2017 *Nat. Nanotechnol.* **12** 425
[6] Cassidy M C *et al* 2017 *Science* **355** 939
[7] Barone A, Rissman P and Russo M 1974 *Rev. Phys. Appl.* **9** 73
[8] Novoselov K S *et al* 2004 *Science* **306** 666
[9] Geim A K 2009 *Science* **324** 1530
[10] Heersche H B *et al* 2007 *Nature* **446** 56

[11] Lee G H, Kim S, Jhi S H and Lee H J 2015 *Nat. Commun.* **6** 6181
[12] Nanda G, Aguilera-Servin J L, Rakyta P, Kormanyos A, Kleiner R, Koelle D, Watanabe K, Taniguchi T, Vandersypen L M K and Goswami S 2017 *Nano Lett.* **17** 3396
[13] Li L *et al* 2014 *Nat. Nanotechnol.* **9** 372
[14] Wang X *et al* 2015 *Nat. Nanotechnol.* **10** 517
[15] Tran V, Soklaski R, Liang Y and Yang L 2014 *Phys. Rev.* B **89** 235319
[16] Xia F, Wang H and Jia Y 2014 *Nat. Commun.* **5** 4458
[17] Qiao J, Kong X, Hu Z, Yang F and Ji W 2014 *Nat. Commun.* **5** 4475
[18] Huang Y *et al* 2016 *Chem. Mater.* **28** 8330
[19] Saito Y and Iwasa Y 2015 *ACS Nano* **9** 3192
[20] Hagymási I, Kormányos A and Cserti J 2010 *Phys. Rev.* B **82** 134516
[21] Wan Z *et al* 2015 *Nat. Commun.* **6** 7426
[22] Stewart W C 1968 *Appl. Phys. Lett.* **12** 277
McCumber D E 1968 *J. Appl. Phys.* **39** 3113
[23] Gubankov V N, Likharev K K and Margolin N M 1972 *Sov. Phys. Solid State* **14** 819
[24] Gross B *et al* 2013 *Phys. Rev.* B **88** 014524
[25] Feshchenko A V *et al* 2017 *Sci. Rep.* **7** 41728
[26] Aizaz A, Bauer P, Grimm T L, Wright N T and Antoine C Z 2007 *IEEE Trans. Appl. Supercond.* **17** 1310
[27] Karimi B and Pekola J P 2018 *Phys. Rev. Appl.* **10** 054048
[28] Rokhinson L P, Liu X and Furdyna J K 2012 *Nat. Phys.* **8** 795
[29] Tinkham M 1996 *Introduction to Superconductivity* (New York: McGraw-Hill)